Transport and boundary scattering in confined geometries: Analytical results

R. A. Richardson and Franco Nori*
Department of Physics, University of Michigan, Ann Arbor, Michigan 48109-1120
(Received 26 March 1993)

We utilize a geometric argument to determine the effects of boundary scattering on the carrier mean free path in samples of various cross sections. Analytic expressions for samples with rectangular and circular cross sections are obtained. We also outline a method for incorporating these results into calculations of the thermal conductivity.

I. INTRODUCTION

There has been considerable interest, in recent years, in the transport properties of various materials in confined geometries (see, e.g., Refs. 1–5). In many such applications, boundary scattering of carriers can be expected to play a significant role. However, when efforts are made to calculate transport quantities, such as the thermal conductivity for small samples, the effect of boundaries is often handled in a fairly simplified fashion. Boundary scattering of phonons, for instance, is typically incorporated by the addition of a constant term to the inverse scattering time for the phonon. The purpose of this paper is to provide a concise expression for the effect of boundaries on transport in small samples which improves upon this basic approach, without invoking the full machinery of the Boltzmann equation. Expressions are obtained for axial transport in samples of circular and rectangular cross section. These results will be applicable to samples which are small enough that the carrier mean free path is on the order of the sample dimensions but not so small that the carrier spectrum is substantially modified from the bulk. In other words, the sample dimensions will be assumed to be much greater than the carrier wavelength.

The method employed is based upon one proposed by Flik and Tien[6] for the calculation of the size effect in thin films. It is also related to a work put forward by Herring[7] in which approximate expressions of the thermoelectric power for some geometries are derived. The Flik and Tien method assumes that, for a carrier of a given frequency, a characteristic bulk mean free path l can be defined which is determined by the other scatterers present in the sample. The goal, then, is to examine how this bulk value of l is modified by the presence of boundaries in the sample. The calculation utilizes the concept of the exchange length l_{ex},[6,8] which is defined as the average distance normal to a plane that a carrier travels after having been scattered within that plane. To be more explicit, we consider a carrier that has undergone a scattering event within a plane that is perpendicular to the direction of net transport which will be referred to from here on as the positive z direction. We now allow the carrier to propagate to the point of its next scattering event, which, in the bulk, is a distance l away. This propagation is assumed to proceed with equal likelihood in all directions. l_{ex} is then defined as the average z component of all possible such propagation vectors, where the average is performed over the hemisphere in the positive z direction. The bulk value of this quantity, l_∞, is determined by the expression,[6]

$$l_\infty = \frac{1}{2\pi}\int_0^{2\pi} d\phi \int_0^{\pi/2} d\theta\, l \sin\theta\, \cos\theta = \frac{l}{2}, \tag{1}$$

where θ is the angle between the vector $\boldsymbol{l}$ and the z axis and ϕ is the angle between the projection of $\boldsymbol{l}$ into the xy plane and the positive x axis.

In the following, we consider the scenario in which the mean free path is on the order of the sample dimensions. For this case, some carriers will strike the boundaries before traveling a full distance l and the exchange length will be correspondingly shorter. We will assume that scattering at the boundaries is *diffuse*, which will be valid when the carrier wavelength is smaller than the characteristic roughness features of the sample surface. We will also consider the sample to be free of grain boundaries, though this calculation could perhaps also be applied to samples whose grains have characteristic geometries which match those investigated here. A geometric analysis will be used to calculate the average exchange length for axial transport in narrow samples (length is assumed infinite) of both circular and rectangular cross section. This quantity will then be related to an effective mean free path l_{eff} which can be used to calculate axial transport coefficients. The calculations presented in the following sections are somewhat lengthy, but we assure the reader that the method pursued, particularly for the rectangular case, is considerably shorter than an approach one might naively take.

II. CALCULATION OF THE EXCHANGE LENGTH

A. Circular cross section

In order to calculate the exchange length for a cylindrical sample, we will initially assume that the excitation can originate with equal likelihood anywhere within a given circular cross section of the sample. The average value of the exchange length in the sample, $\tilde{l}_{ex}$, will

then be obtained by averaging l_{ex} (which is itself an average over a hemisphere of solid angle) over the entire cross section. The geometry to be considered is shown in Fig. 1. We consider an excitation originating at some point a distance ρ from the center of the cross section of radius R and propagating in a random direction within the hemisphere of solid angle whose base is normal to the positive z direction. The quantity θ is defined as the angle between the propagation vector $\boldsymbol{l}$ and the z axis, and ϕ is the angle between the radius along which the origination point is located and the projection of $\boldsymbol{l}$ into the plane of the cross section. Note that $\boldsymbol{l}$ may or may not have length l, depending upon whether or not it is truncated by a boundary. We will also find it useful to define the quantity $s(\rho,\phi)$ as the length of the segment within the cross-section plane which begins at the origination point and extends to the sample boundary in the direction of ϕ (see Fig. 1). This will be the length of the projection of $\boldsymbol{l}$ into the plane of the cross section for the case in which the carrier hits the wall before traveling a full mean free path l. The average exchange length will then be given by the expression

$$\tilde{l}_{ex} = \frac{2}{\pi R^2}\int_0^R d\rho\,\rho\int_0^\pi d\phi\int_0^{\pi/2} d\theta\sin\theta\, l_z(\rho,\phi,\theta), \qquad (2)$$

where l_z is the z component of the propagation vector heading in the (θ,ϕ) direction and ϕ has only been integrated over half its range for symmetry reasons. In the above, an integration over the polar angle ξ within the cross-section plane has already been performed since l_z does not depend on it.

We now need to consider the separate cases in which $\boldsymbol{l}$ does and does not hit the wall. For a given ρ and ϕ, $\boldsymbol{l}$ will hit within the range $\theta^* < \theta < \pi/2$ where θ^* is given by

$$\theta^* = \sin^{-1}\left(\frac{s(\rho,\phi)}{l}\right).$$

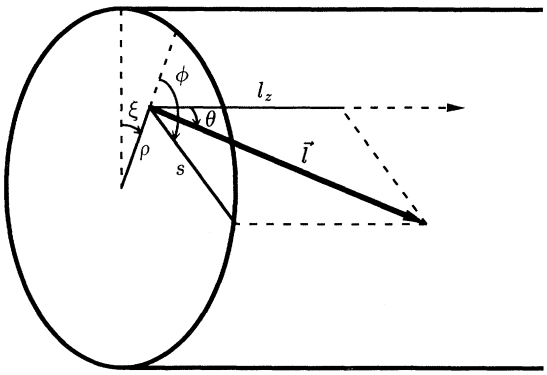

FIG. 1. Schematic showing the geometry relevant for the calculation of the exchange length for a wire of circular cross section. The case pictured is that for which $\boldsymbol{l}$ hits the boundary. Note however that the quantity s is always defined as the segment within the cross-section plane that stretches from the origination point to the boundary, regardless of whether or not $\boldsymbol{l}$ actually hits the boundary.

The corresponding expressions for l_z for these two cases are given by

$$l_z(\rho,\phi,\theta) = \begin{cases} l\cos\theta & \text{if } 0<\theta<\theta^* \\ s(\rho,\phi)\cot\theta & \text{if } \theta^*<\theta<\pi/2. \end{cases} \qquad (3)$$

We will also encounter situations when $l < 2R$, where, for certain ranges of ρ and ϕ, $s(\rho,\phi) > l$. In these cases, $\boldsymbol{l}$ *never* hits the wall for *any* θ. How these ranges are determined will be examined more fully below.

We are now in a position to evaluate the θ integral. We will distinguish between the two cases described above, i.e., $\boldsymbol{l}$ *sometimes* hits the wall [l_z is described by Eq. (3)] and, $\boldsymbol{l}$ *never* hits the wall ($l_z = l\cos\theta$ for all θ). These will be referred to hereafter as the SH and NH regimes. The result of the θ integration is

$$\int_0^{\pi/2} d\theta\sin\theta\, l_z(\rho,\phi,\theta) = \begin{cases} l/2 & \text{never hits (NH)} \\ s(\rho,\phi) - s(\rho,\phi)^2/2l & \text{sometimes hits (SH).} \end{cases} \qquad (4)$$

To proceed further, we must consider the relative magnitudes of l and R. There are two relevant possibilities, $l \geq 2R$ and $l < 2R$. We will consider the simpler of these two cases first, $l \geq 2R$. In this regime, one can see that, with regards to the θ integration, we will always "sometimes hit" the wall, for all possible values of ρ and ϕ. After performing the θ integration, the expression for $\tilde{l}_{ex}$ becomes

$$\tilde{l}_{ex} = \frac{2}{\pi R^2}\int_0^R d\rho\,\rho\int_0^\pi d\phi\left(s(\rho,\phi) - \frac{s(\rho,\phi)^2}{2l}\right), \qquad (5)$$

where, as can be determined from the geometry of the problem,

$$s(\rho,\phi) = (R^2 - \rho^2\sin^2\phi)^{1/2} - \rho\cos\phi. \qquad (6)$$

It is possible to integrate the $-s^2/2l$ term in the order written above (ϕ first), but it can be shown that the s term must be evaluated by performing the ρ integration first to achieve an analytical solution. These operations yield the following result:

$$\tilde{l}_{ex} = \frac{8R}{3\pi} - \frac{R^2}{2l}, \quad l \geq 2R. \qquad (7)$$

The case where $l < 2R$ is somewhat more involved. Here we must distinguish between those regions of (ρ,ϕ) space where we are in the SH regime with regards to the θ integration and those where we are in the NH regime. The following results will be derived upon the assumption that $l < R$. The remaining case, $R < l < 2R$, can be shown, though it is not readily apparent, to yield results identical to the $l < R$ case and we will therefore spare the reader their derivation. Assuming, then, that $l < R$,

one can see that in the region where $\rho < R - l$, $\boldsymbol{l}$ never hits the wall, regardless of ϕ and θ. For $\rho \geq R - l$, on the other hand, we can be either in the SH or NH regime, depending upon the value of ρ and ϕ. It can be seen that, given a ρ greater than $R - l$, the angle ϕ^* for which we cross over from the SH to the NH regime is determined by the condition that $s(\rho, \phi^*) = l$. The geometry for this situation is illustrated in Fig. 2. Using this condition, it can be shown that

$$\phi^* = \pi - \cos^{-1}\left(\frac{\rho^2 + l^2 - R^2}{2l\rho}\right).$$

Summarizing these considerations for the $l < R$ case, we arrive at the expression

$$\tilde{l}_{\rm ex} = \frac{2}{\pi R^2}\left\{ \int_{R-l}^{R} d\rho\,\rho\left[\int_0^{\phi^*} d\phi\,\left(s(\rho,\phi) - \frac{s(\rho,\phi)^2}{2l}\right) + \int_{\phi^*}^{\pi} d\phi\,\frac{l}{2}\right] + \int_0^{R-l} d\rho\rho \int_0^{\pi} d\phi\,\frac{l}{2}\right\}. \tag{8}$$

The NH terms, where the ϕ integrand is $l/2$, as well as the term involving $-s^2/2l$, can be evaluated as presented above. However, the "s term" t_s, as given by

$$t_s = \frac{2}{\pi R^2}\int_{R-l}^{R} d\rho\,\rho \int_0^{\phi^*} d\phi\, s(\rho,\phi), \tag{9}$$

cannot be evaluated in the integration order shown, since the ϕ integral is elliptic. So, as in the $l > 2R$ case, we must reverse the order of integration and approach the ρ integral first. This procedure is less straightforward than the previous case, however, due to the fact that the upper limit of the ϕ integral in Eq. (9) is ρ dependent.

We must reconsider the problem from the perspective of integrating over ρ for constant ϕ. The relevant geometry for this case is presented in Figs. 3(a) and 3(b). The goal is to determine the regions of phase space where we are in the SH regime, as this is the only region which involves the s term that we seek to evaluate. If we first examine the different ranges of ϕ, we can see that for large values of this angle, we will never hit the boundary for any ρ or θ. The critical angle ϕ_2^* above which this will be the case is determined by the condition that $s(R, \phi_2^*) = l$ [see Fig. 3(a)] and can be shown to be given by $\phi_2^* = \pi - \cos^{-1}(\frac{l}{2R})$. Now, directing our attention to the different possible ranges of ρ, one can see that for $\phi < \phi_2^*$, we will be in the NH regime for small ρ and will cross over to the SH regime at a critical value ρ^*. The determining condition for this crossover will again be that $s(\rho^*, \phi) = l$ [see Fig. 3(b)], which leads to the result

$$\rho^* = (R^2 - l^2 \sin^2\phi)^{1/2} - l\cos\phi.$$

These various considerations yield the proper expression for the s term with the integration order reversed,

$$t_s = \frac{2}{\pi R^2}\int_0^{\phi_2^*} d\phi \int_{\rho^*}^{R} d\rho\,\rho\, s(\rho,\phi), \tag{10}$$

where ϕ_2^* and ρ^* are given above. This expression can now be evaluated and, when combined with the results for the other terms obtained from Eq. (8), gives the total result for the $l < 2R$ case:

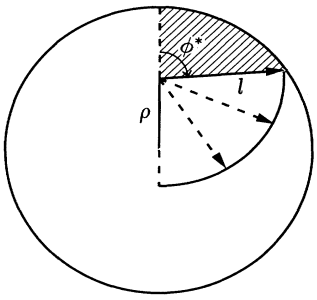

FIG. 2. Schematic of the various regimes when $l < R$ and $R - l < \rho < R$. The angle ϕ^* is defined by the condition that $s(\rho, \phi^*) = l$. For angles greater than ϕ^*, $\boldsymbol{l}$ never hits the boundary. Arrows indicate possible orientations of the vector $\boldsymbol{l}$ when $\theta = \pi/2$.

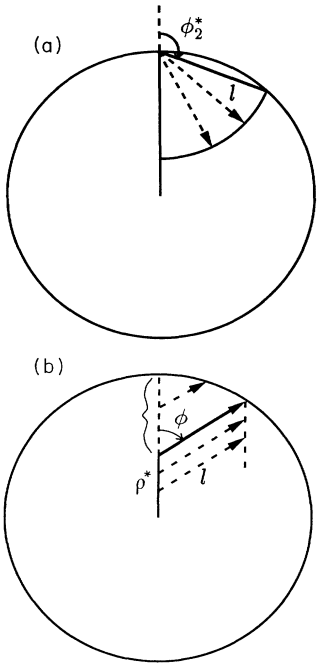

FIG. 3. (a) Schematic indicating how the angle ϕ_2^*, above which $\boldsymbol{l}$ never hits the boundary for any ρ, is determined. When $\phi = \phi_2^*$, $s(R, \phi_2^*) = l$. (b) Schematic indicating how ρ^*, above which $\boldsymbol{l}$ sometimes hits the boundary, is determined for a given ϕ. When $\rho = \rho^*$, $s(\rho^*, \phi) = l$. Arrows indicate possible orientations of the vector $\boldsymbol{l}$ when $\theta = \pi/2$ for varying ρ and fixed ϕ. The relevant region for the ρ integration portion of the s term is indicated by the bracket.

$$\tilde{l}_{\rm ex} = \frac{8R}{3\pi} - \frac{R^2}{2l} + \frac{l}{\pi}\cos^{-1}\left(\frac{l}{2R}\right) + \frac{R^2}{2\pi l}\cos^{-1}\left(\frac{l^2}{2R^2}-1\right) - \frac{(4R^2-l^2)^{1/2}}{\pi}\left(\frac{13}{12}+\frac{l^2}{24R^2}\right), \quad l<2R\ . \tag{11}$$

It is interesting to note that the $-s^2/2l$ term *cannot* be integrated in a straightforward fashion with the ρ and ϕ integrations reversed, so both perspectives are necessary for a complete solution to the problem.

B. Rectangular cross section

We now turn our attention to samples of rectangular cross section. The general expression for $\tilde{l}_{\rm ex}$ is quite analogous to the circular case and is given by

$$\tilde{l}_{\rm ex} = \frac{2}{\pi ab}\int_0^{a/2} dx \int_0^{b/2} dy \int_0^{2\pi} d\phi \int_0^{\pi/2} d\theta \sin\theta \times l_z(x,y,\phi,\theta), \tag{12}$$

where a and b are the lengths of the two sides and the integration is performed over only the bottom-left quarter of the cross section for symmetry reasons. The bottom-left corner is chosen as the origin of x and y and the a side lies along the x direction. We will define $s(x,y,\phi)$ in a manner analogous to the previous case, i.e., the distance from the origination point to the wall in the ϕ direction, and point out that the results of the θ integration can again be divided into SH and NH regimes with the results shown in Eq. (4) applicable here as well. The expression for s will depend upon which boundary we are relating it to and, for the bottom wall, for instance, is given by

$$s(x,y,\phi) = y\sec\phi. \tag{13}$$

The integrations over ϕ, x, and y require careful consideration to determine the regions of (x,y,ϕ) space where we are in the SH or NH regimes. We will find that, as before, the makeup of these regions depends on the relative magnitudes of l, a, and b. We first examine the case when $l > \sqrt{a^2+b^2}$. This is the simplest scenario because we are in the SH regime for all x, y, and ϕ. The geometry for this case is illustrated in Figs. 4 and 5. For a given origination point (x,y), we have to consider four ranges of ϕ integration: $\phi_1 \to \phi_2$, $\phi_3 \to \phi_4$, $\phi_5 \to \phi_6$, and $\phi_7 \to \phi_8$, corresponding to hitting the bottom, left, top, and right walls, respectively (see Fig. 4). For the bottom wall, ϕ is measured with respect to the vertical through the origination point, with ϕ_1 in the negative direction and ϕ_2 in the positive direction. The counterclockwise directional convention is chosen because $\boldsymbol{l}$ is directed into the plane of the paper. To avoid ambiguity in the evaluation of inverse tangents, which appear frequently in the calculation, a new zero of ϕ is defined for each side, with, for example, the zero with respect to the left side taken as the horizontal to the left of the origination point.

We are now prepared to undertake the integration over the full range of ϕ. This task can be considerably simplified, however, by taking into account the symmetry of the problem. This process is illustrated schematically in Fig. 5. We begin by treating the contributions from the top and bottom, hereafter referred to as the "top/bottom" terms, separately from the sides. We will find that the latter can be related to the former by symmetry. Next, we note that the integration over the *bottom-left* quarter of our cross section of those ϕ's which will place us in the region where scattering will occur from the *top* boundary, i.e., $\phi_5 \to \phi_6$, is equivalent, by a 180° rotation, to an integration over the *top-right* quarter of the cross section of those ϕ's where scattering will occur from the *bottom* of the sample, i.e., $\phi_1 \to \phi_2$. The part of our integral which accounts for scattering from the top and bottom boundaries then becomes

$$\left[\int_0^{a/2} dx \int_0^{b/2} dy + \int_{a/2}^{a} dx \int_{b/2}^{b} dy\right] \int_{\phi_1(x,y)}^{\phi_2(x,y)} d\phi \left(s(x,y,\phi) - \frac{s(x,y,\phi)^2}{2l}\right). \tag{14}$$

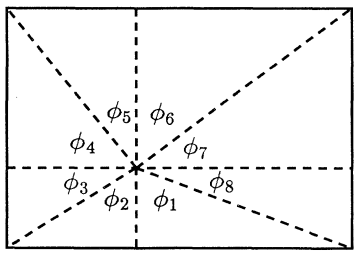

FIG. 4. Diagram indicating the various values of ϕ which are used in the determination of the exchange length in a sample of rectangular cross section.

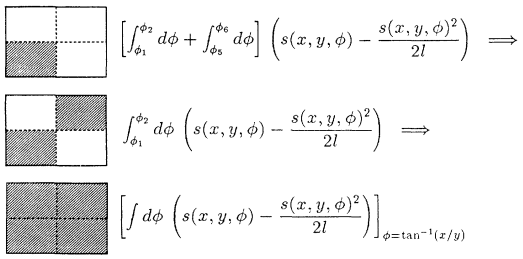

FIG. 5. Schematic representation of the symmetry processes used to simplify the calculation of the average exchange length. The rectangular diagrams represent double integrals in the (x,y) plane over the shaded regions.

The next simplification occurs as a result of an additional symmetry. It can be shown that when the ϕ integral is evaluated at its lower limit ϕ_1, one obtains the same expression as when it is evaluated at the upper limit ϕ_2, provided that the ϕ_1 expression is subjected to a change of variables which changes the region of integration in (x,y) space. Specifically, the appropriate region is obtained by taking the original region and reflecting it about the line $x = a/2$. The benefit of this operation is that we reduce an expression which involves two terms, the ϕ integral evaluated at its upper and lower limits, to one involving only one term, simply by changing the region of (x,y) integration. In particular, we arrive at an expression which is the ϕ integral evaluated at its upper limit ϕ_2, where the region of (x,y) integration is the one given in Eq. (14) *plus* its reflection about the line $x = a/2$ (see Fig. 5). This leads to the following expression for the top/bottom terms:

$$\int_0^a dx \int_0^b dy \left[\int d\phi \left(s(x,y,\phi) - \frac{s(x,y,\phi)^2}{2l} \right) \right]_{\phi=\phi_2(x,y)}, \tag{15}$$

where $\phi_2(x,y) = \tan^{-1}(x/y)$ and $s(x,y,\phi)$ is given by Eq. (13). One can go through the same logic for the scattering contribution from the sides and it can be seen, by making the substitution $x \to y$ and $y \to x$, that the expression obtained is identical to the one above with the exception that the upper limits of the x and y integrals are reversed. Summing these two contributions and performing the integrations we arrive at the total expression for the case in which $l > \sqrt{a^2+b^2}$,

$$\tilde{l}_{\rm ex} = \frac{a}{\pi} \ln\left(\frac{b+\sqrt{a^2+b^2}}{a} \right) + \frac{b}{\pi} \ln\left(\frac{a+\sqrt{a^2+b^2}}{b} \right) + \frac{1}{3\pi ab}\left[a^3+b^3-(a^2+b^2)^{3/2} \right] - \frac{ab}{2\pi l} \equiv H. \tag{16}$$

The symmetry considerations illustrated here are not essential for performing the calculation above, but they become increasingly useful as one examines more complicated cases. Specifically, let us consider the case when $l < a,b$. As in the circular calculation, we will derive the results for a limited portion of this range and then demonstrate that they are applicable for the entire range. We will initially require l to be less than $a/2$ and $b/2$. Taking, once again, the region of (x,y) integration to be the lower-left quarter of the cross section, one can see that $\boldsymbol{l}$ can only hit the bottom and left sides. The task is, as before, to discern which regions of (x,y,ϕ) space place us in the SH regime and which place us in the NH regime. The simplest way of visualizing this is to consider a circle of radius l, with its center located at various points (x,y) within the lower-left quarter, and to examine the manner in which it intersects the boundaries. We shall be particularly interested in the bottom wall, as the sides can be related to it by symmetry arguments. The relevant regions are shown in Fig. 6. In region I, within a radius l from the bottom-left corner, our circle intersects the bottom wall exactly once. For points within this region, when one considers the integration of ϕ over the bottom wall (i.e., from ϕ_1 to ϕ_2), it can be seen that we are in the NH regime from ϕ_1 to some angle ϕ_1^* and in the SH regime from ϕ_1^* to ϕ_2. ϕ_1^* is determined by the condition that $s(x,y,\phi_1^*) = l$ and is given by

$$\phi_1^* = -\tan^{-1}\left(\frac{\sqrt{l^2-y^2}}{y} \right). \tag{17}$$

For points in region II, which have $y < l$ but are farther than l from the corner, our circle intersects the bottom wall in two places, ϕ_1^* and ϕ_2^*. ϕ_1^* is as defined above and $-\phi_2^* = \phi_1^*$. In this region, we find as we integrate ϕ across the bottom wall, that we are in the SH regime for $\phi_1^* < \phi < \phi_2^*$ and in the NH regime elsewhere. Finally, in region III, where $y > l$, our circle does not intersect the bottom wall at all and the NH expression applies to the entire ϕ integration.

Now let us consider the top wall. It is clear that the NH expression applies as we integrate from ϕ_5 to ϕ_6 for origination points anywhere in the lower-left quarter of the cross section. We can now apply the symmetry manipulations described for the $l > \sqrt{a^2+b^2}$ case to the present scenario. First, we rotate the "top" integration (ϕ_5 to ϕ_6) by 180° to convert it to an integration over the upper-right quarter from ϕ_1 to ϕ_2. We can now combine this contribution with the integral obtained for region III, as they both represent integrations from ϕ_1 to ϕ_2 where the NH expression holds for the entire range. The various ϕ integrals we need to evaluate, then, are shown in Fig. 7(a), with their respective regions of (x,y) integration represented pictorially. These integrals represent the total contribution from integrations over the top and bottom walls to our expression for $\tilde{l}_{\rm ex}$, i.e., the top/bottom terms. At this stage we can divide up the ϕ integrals into their constituent upper and lower limit parts, and by performing the type of variable substitutions and accompanying (x,y) integration region reflections discussed for the previous case reduce the problem to that shown schematically in Fig. 7(b). The top/bottom contributions C derived from Fig. 7(a) are indicated by the diagrams on the left. Those on the right represent the contributions from the sides. To illustrate how these schematics are converted to mathematical expressions, we will write out the top/bottom terms [those indicated by the diagrams on the left in Fig. 7(b)] explicitly:

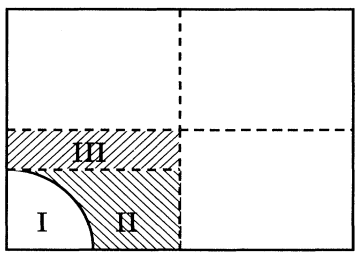

FIG. 6. Diagram indicating the various regions in the (x,y) plane which must be treated in the calculation of the average exchange length. In region I, a circle of radius l intersects the bottom wall once. In region II, a circle of radius l intersects the bottom wall twice and in region III there is no intersection. The curve in the figure has radius l.

$$C = \int_0^l dx \int_0^{\sqrt{l^2-x^2}} dy \left[\int d\phi \left(s(x,y,\phi) - \frac{s(x,y,\phi)^2}{2l} \right) \right]_{\phi=\tan^{-1}(x/y)}$$
$$+ \int_0^l dy \int_{\sqrt{l^2-y^2}}^a dx \left[\int d\phi \left(s(x,y,\phi) - \frac{s(x,y,\phi)^2}{2l} - \frac{l}{2} \right) \right]_{\phi=\tan^{-1}(\sqrt{l^2-y^2}/y)}$$
$$+ \left[\int_0^a dx \int_0^b dy - \int_0^l dx \int_0^{\sqrt{l^2-x^2}} dy \right] \left[\int d\phi \frac{l}{2} \right]_{\phi=\tan^{-1}(x/y)}, \tag{18}$$

where, again, $s(x,y,\phi)$ is given by Eq. (13). An analogous expression describes the side wall contributions. The only changes are in the limits of the (x,y) integrations, and these are indicated by the diagrams on the right in Fig. 7(b). Combining all contributions and performing the integrations it can be shown that the total expression for the case where $l < a, b$ is

$$\tilde{l}_{ex} = \frac{l}{2} - \frac{(a+b)l^2}{3\pi ab} + \frac{l^3}{12\pi ab} \equiv F. \tag{19}$$

Recall that the results above were derived for the case in which $l < a/2, b/2$. The case where $b/2 < l < b$ appears, on the surface, to be quite different, since, in an analysis of the type described in Fig. 6, one would need to consider the possibility of hitting the top wall. However, an examination of the forms of the integration regions depicted in Fig. 7(b) reveals that they undergo no meaningful change until l becomes greater than b. This is one of the benefits of the manipulations which result in Fig. 7(b); they reveal the fundamental equivalence of apparently disparate cases. The other principal benefit of the technique is that it obviates the need to extensively evaluate the various SH and NH regions for other, *nonidentical* cases since the diagrams shown in Fig. 7(b) can be logically extended to other regimes. The case where $b < l < a$ for instance, is shown in Fig. 8(a). We note that the difference between the top/bottom diagrams and the side diagrams for this case results in an asymmetrical dependence of $\tilde{l}_{ex}$ on a and b. Performing the integrations indicated in the figure, we find that

$$\tilde{l}_{ex} = F + G(b), \tag{20}$$

where

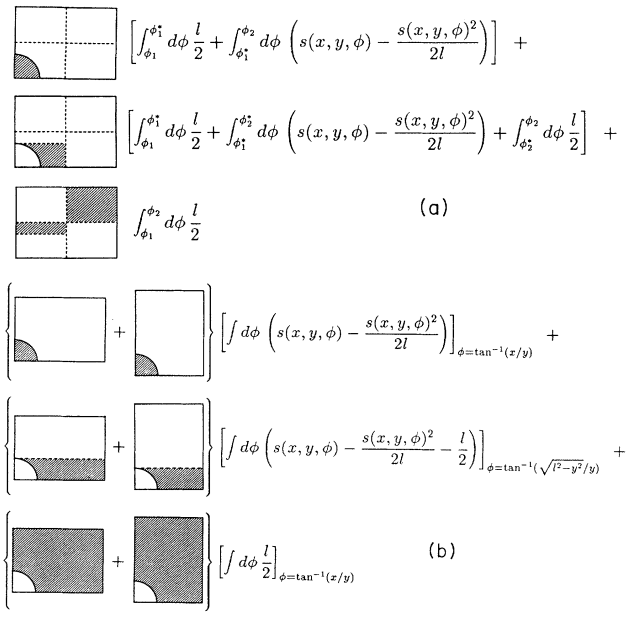

FIG. 7. (a) Schematic representation of the various terms involved in the calculation of the contribution from the top and bottom walls to the exchange length for the case in which $l < a/2, b/2$. The rectangular diagrams represent integrations in the (x,y) plane over the shaded regions. (b) Terms used to calculate the average exchange length $\tilde{l}_{ex}$ after symmetry manipulations have been applied. The leftmost diagram in each term represents the contribution from the top and bottom walls and the rightmost diagram represents the contribution from the side walls. These terms must be multiplied by a prefactor to yield the final result for $\tilde{l}_{ex}$. The curves in the diagrams have radius l and are centered at the lower left corner.

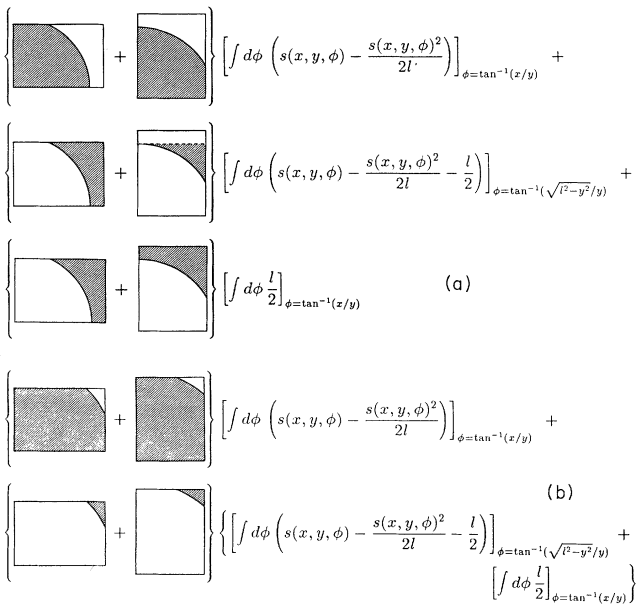

FIG. 8. (a) Terms used in the calculation of the average exchange length for the case in which $b < l < a$. The diagrams representing the (x,y) integrations can be seen to be logical extensions of the previous case. Again, the curves have radius l. (b) Terms used in the calculation of the average exchange length for the case in which $b, a < l < \sqrt{a^2+b^2}$.

$$G(q) \equiv -\frac{(q-l)^4}{12\pi abl} + \frac{q}{\pi}\ln\left(\frac{l}{q} + \sqrt{(l/q)^2-1}\right) - \frac{l}{\pi}\cos^{-1}\left(\frac{q}{l}\right) + \frac{(l^2-q^2)^{3/2}}{3\pi ql} \tag{21}$$

and F is as defined in Eq. (19).

The final case to consider is that for which $a, b < l < \sqrt{a^2+b^2}$. The appropriate diagrams are shown in Fig. 8(b) and they lead to the result

$$\tilde{l}_{\rm ex} = F + G(a) + G(b). \tag{22}$$

One final remark: the case where $l > \sqrt{a^2+b^2}$ which we analyzed first can now be seen to result from the final possible extension of the diagrams shown in Figs. 7 and 8. The shaded regions on the top line of Fig. 8(b) expand to encompass the entire rectangles and the terms on the second line go to zero.

III. BOUNDARY ORIGINATION

All of the above expressions, for both the circular and rectangular cases, were derived on the assumption of uniform origination, i.e., we assume that the excitation can originate anywhere within the cross section with equal likelihood. Recalling the physical interpretation of the exchange length, however, we note that the excitations we are considering are those that have just undergone a scattering event within the cross-section plane. As pointed out in Ref. 6, when the mean free path of the excitation becomes much longer than the sample dimensions, the excitation becomes increasingly likely to scatter on a boundary and our assumption of uniform origination needs to be replaced with a boundary origination description. The expressions appropriate for boundary origination are as follows.

Circular:

$$\tilde{l}_{\rm ex} = \frac{2}{\pi}\int_0^{\pi/2} d\phi\left(s(R,\phi) - \frac{s(R,\phi)^2}{2l}\right) = \frac{4R}{\pi} - \frac{R^2}{l}\ . \tag{23}$$

Rectangular:

$$\begin{aligned}\tilde{l}_{\rm ex} &= \frac{4}{\pi(a+b)}\left\{\int_0^a dx\left[2\int_0^{\tan^{-1}(b/x)} d\phi\,(s - s^2/2l) + \int_{-\tan^{-1}\left(\frac{x}{b}\right)}^{\tan^{-1}\left(\frac{a-x}{b}\right)} d\phi\,(s - s^2/2l)\right]\right. \\ &\quad \left. + \int_0^b dy\left[2\int_0^{\tan^{-1}(a/y)} d\phi\,(s - s^2/2l) + \int_{-\tan^{-1}\left(\frac{y}{a}\right)}^{\tan^{-1}\left(\frac{b-y}{a}\right)} d\phi\,(s - s^2/2l)\right]\right\} \\ &= \frac{2}{\pi(a+b)}\left[\left(\frac{a^2}{2}+ab\right)\ln\left(\frac{b+\sqrt{a^2+b^2}}{a}\right) + \left(\frac{b^2}{2}+ab\right)\ln\left(\frac{a+\sqrt{a^2+b^2}}{b}\right)\right] \\ &\quad + \frac{(a^2+b^2)}{\pi(a+b)} - \frac{\sqrt{a^2+b^2}}{\pi} - \frac{ab}{\pi l} \equiv J\ .\end{aligned} \tag{24}$$

TABLE I. Summary of the equations for $\tilde{l}_{\rm ex}$ for the various different geometries and the various ranges of the mean free path l. R is the radius for the circular case, and a and b are the lengths of the sides for the rectangular case, with b taken to be the shorter of the two. d is equal to $\sqrt{a^2+b^2}$.

Cross section	Range	$\tilde{l}_{\rm ex}$
Circle	$l < 2R$	$\frac{8R}{3\pi} - \frac{R^2}{2l} + \frac{l}{\pi}\cos^{-1}\left(\frac{l}{2R}\right) + \frac{R^2}{2\pi l}\cos^{-1}\left(\frac{l^2}{2R^2}-1\right) - \frac{(4R^2-l^2)^{1/2}}{\pi}\left(\frac{13}{12}+\frac{l^2}{24R^2}\right)$
	$l \geq 2R$	$\frac{8R}{3\pi} - \frac{R^2}{2l} + \exp(-8R/l)\left(\frac{4R}{3\pi} - \frac{R^2}{2l}\right)$
Rectangle	$l < b$	$F(a,b)$
	$b \leq l < a$	$F(a,b) + G(b,a)$
	$a \leq l < d$	$F(a,b) + G(a,b) + G(b,a)$
	$l \geq d$	$H + \exp(-4d/l)(J - H)$
Square	$l < a$	$F(a,a)$
	$a \leq l < \sqrt{2}a$	$F(a,a) + 2G(a,a)$
	$l \geq \sqrt{2}a$	$\frac{a}{\pi}\left[2 + \exp(-\frac{4\sqrt{2}a}{l})\right]\left[\ln(1+\sqrt{2}) + (1-\sqrt{2})/3\right] - \frac{a^2}{2\pi l}\left[1 + \exp(-\frac{4\sqrt{2}a}{l})\right]$

$$F(p,q) \equiv \frac{l}{2} - \frac{(p+q)l^2}{3\pi pq} + \frac{l^3}{12\pi pq}$$

$$G(p,q) \equiv -\frac{(p-l)^4}{12\pi pql} + \frac{p}{\pi}\ln\left(\frac{l}{p} + \sqrt{(l/p)^2-1}\right) - \frac{l}{\pi}\cos^{-1}\left(\frac{p}{l}\right) + \frac{(l^2-p^2)^{3/2}}{3\pi pl}$$

$$H \equiv \frac{a}{\pi}\ln\left(\frac{b+d}{a}\right) + \frac{b}{\pi}\ln\left(\frac{a+d}{b}\right) + \frac{1}{3\pi ab}\left[a^3+b^3-d^3\right] - \frac{ab}{2\pi l}$$

$$J \equiv \frac{2}{\pi(a+b)}\left[\left(\frac{a^2}{2}+ab\right)\ln\left(\frac{b+d}{a}\right) + \left(\frac{b^2}{2}+ab\right)\ln\left(\frac{a+d}{b}\right)\right] + \frac{d^2}{\pi(a+b)} - \frac{d}{\pi} - \frac{ab}{\pi l}$$

The appropriate procedure[6] is to match these solutions to those for uniform origination at large l's. This can be accomplished by a simple process which is as follows. If we wish the uniform solution, which we will call solution S_1, to apply at some $l = l'$ and we wish the boundary solution, which we will call solution S_2, to apply for large l, the matched solution S_m may be derived by the expression,

$$S_m = S_1 + \exp(-ml'/l)(S_2 - S_1), \tag{25}$$

where m is a matching parameter. We will take l' to be $2R$ for the circular case and $\sqrt{a^2 + b^2}$ for the rectangular case. The matched solutions then become for the circular case,

$$\tilde{l}_{\rm ex} = \frac{8R}{3\pi} - \frac{R^2}{2l} + \exp(-m2R/l)\left(\frac{4R}{3\pi} - \frac{R^2}{2l}\right), \quad l \geq 2R \tag{26}$$

and for the rectangular case,

$$\tilde{l}_{\rm ex} = H + \exp(-md/l)[J - H] , \tag{27}$$

where $d = \sqrt{a^2 + b^2}$, and H and J are defined by Eqs. (16) and (24), respectively. These forms result in small discontinuities at $l = l'$ when they are combined with the solutions for $l < l'$ derived in the previous sections, Eqs. (11) and (22). If the matching parameter m is chosen to be four, this discontinuity is less than 1.5%. It should be noted that, for the rectangular case when $a \gg b$, we can expect to be largely in the boundary origination regime before l exceeds the length of the diagonal. The above equation does not allow for this possibility and is therefore most applicable to cases in which a is not too different from b. For samples where one dimension is much larger than the other, we refer the reader to the results of Ref. 6 where an expression for thin films is derived.

IV. DISCUSSION

For the sake of clarity, the results for all the cases examined are summarized in Table I. Also included is the square subcase of the rectangular expression.

These expressions can now be used to aid in the calculation of transport quantities in samples where boundary scattering is expected to play a role. We will examine the thermal transport in particular. In the kinetic theory approximation, the thermal conductivity is given by

$$\kappa = \tfrac{1}{3}Cvl, \tag{28}$$

where C is the contribution to the specific heat from the carrier in question and v is the carrier velocity. Now, in Ref. 6, it is asserted that, within this approximation, the transport κ_z along the z axis in a sample of confined geometry can be obtained from the bulk thermal conductivity κ_∞ and the exchange length along that axis by the expression

$$\kappa_z = \kappa_\infty \frac{\tilde{l}_{\rm ex}}{l/2}. \tag{29}$$

It can easily be seen that this is equivalent to writing κ_z as a function of l as

$$\kappa_z(l) = \kappa_\infty(l_{\rm eff}) \tag{30}$$

with

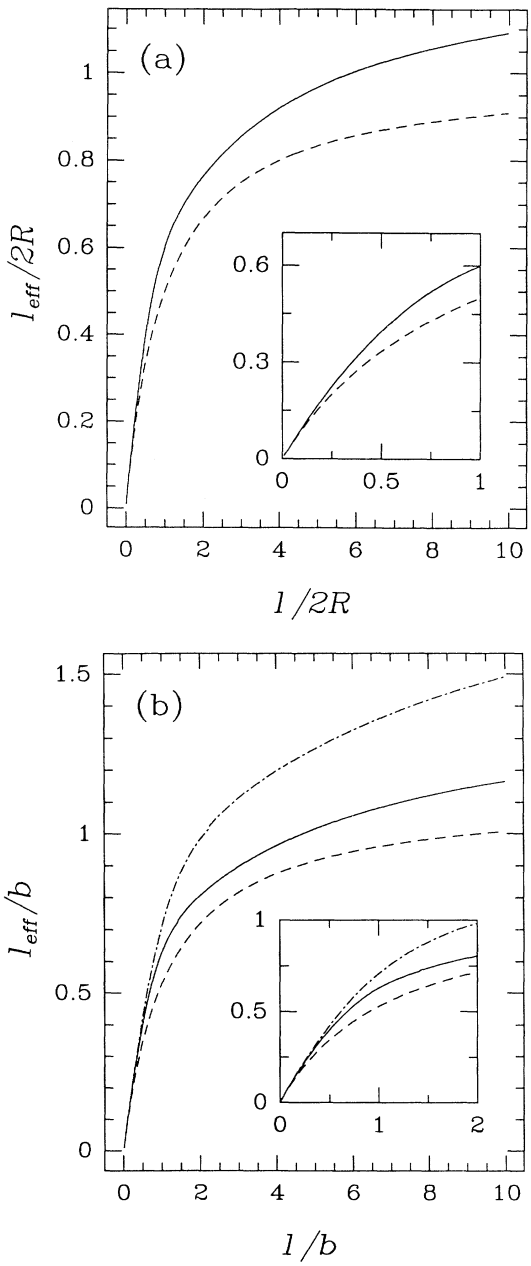

FIG. 9. (a) Plot of the reduced effective mean free path vs the reduced bulk mean free path for the circular case. The solid line indicates the results when the exchange length method is used while the dashed line indicates Casimir's results using Eq. (34) with $\alpha = 1$. The inset shows a blow up of the low l region and has the same axes as the surrounding plot. (b) Results for the rectangular case. The solid line shows the result for $a = b$ and the dot-dashed line represents the case in which $a = 2b$. As in (a), the dashed line shows the result from Eq. (34) with $\alpha = 1.12$. Inset is as in (a).

$$l_{\text{eff}} = 2\tilde{l}_{\text{ex}}. \tag{31}$$

In other words, the transport in the small sample can be obtained from the expression for the bulk transport by replacing l in the latter expression with l_{eff} as defined above.

Because of the simple geometric nature of this argument, it is plausible that this sort of analysis can be applied to more sophisticated treatments of the thermal conductivity as well. For instance, in the case of phonon transport, the thermal conductivity is often written in the Debye approximation as an integral over phonon frequencies;[9]

$$\kappa_p(T) = \frac{k_B}{2\pi^2 v}\left(\frac{k_B}{\hbar}\right)^3 T^3 \int_0^{\theta_D/T} dx\, \frac{x^4 e^x}{(e^x-1)^2}\,\tau(T,x), \tag{32}$$

where x is the reduced phonon frequency $\hbar\omega/k_BT$, k_B is the Boltzmann constant, θ_D is the Debye temperature, and $\tau(T,x)$ is the frequency dependent scattering time. The total inverse scattering time $\tau(T,x)^{-1}$ is usually expressed as a summation of the inverse scattering times from scatterers of various types, e.g., point defects, phonon-phonon umklapp processes, etc. Within this context, the effect of boundaries is typically incorporated by adding a frequency-independent term to this total of the form[10]

$$\tau_b^{-1} = v/\alpha d, \tag{33}$$

where d represents the sample dimension and α is a geometrical factor.

We propose that greater accuracy may be achieved from calculations involving Eq. (32) by omitting the boundary scattering term in the total inverse scattering time and utilizing the above equations for the exchange length to modify the mean free path instead. The proposed procedure is as follows: the factor τ in Eq. (32) can readily be replaced by $l(x,T)/v$, at which point the integration can be seen to be over the frequency-dependent mean free path multiplied by another x-dependent factor. For each such mean free path $l(x,T)$, a value of $\tilde{l}_{\text{ex}}$ can be derived by using the equation appropriate for the geometry of the particular sample under investigation. Each $l(x,T)$ in the integral can then be replaced by an $l_{\text{eff}}(x,T) = 2\tilde{l}_{\text{ex}}(x,T)$ as indicated in Eq. (31). The proper, boundary limited value of the thermal conductivity is then obtained by integrating over the $l_{\text{eff}}(x,T)$, with the other factors in Eq. (32) left unaltered.

The dependence of l_{eff} on l for various geometries is shown in Fig. 9. Also shown in Fig. 9 is the result when l_{eff} is determined by the expression

$$l_{\text{eff}} = \left(\frac{1}{\alpha d} + \frac{1}{l}\right)^{-1}, \tag{34}$$

where α is taken to be 1 for the circular case and 1.12 for the square case.[10] This expression results from making the assumptions summarized in Eq. (33), i.e., the effect of boundary scattering is addressed by adding a constant term to the total inverse scattering time. One can see that the discrepancy is approximately 20% in the region where l is close to the sample dimensions. While this error is not terribly large for the square and circular cases, Eq. (34) cannot be used at all for the rectangular geometry, where the sample cannot be characterized by a single dimension.

V. CONCLUSIONS

In summary, we have presented analytical expressions for the effects of boundary scattering in samples where the bulk carrier mean free path is determined by other scatterers present. Results are derived for axial transport in long, narrow samples of circular and rectangular cross section, where scattering at the boundaries is diffuse. The results are incorporated into a definition of an effective mean free path for axial transport which can be used to calculate coefficients such as the thermal conductivity. Though we have focused on thermal transport in the present work, the expressions derived here could be of use in the examination of a variety of transport phenomena in confined geometries.

ACKNOWLEDGMENTS

F.N. acknowledges partial support from GE, a Rackham grant, the NSF through Grant No. DMR-90-01502, and SUN Microsystems.

*To whom correspondence should be addressed.

[1]F. Rossi *et al.*, Phys. Rev. B **47**, 1695 (1993).
[2]J. Seyler and M. N. Wybourne, Phys Rev. Lett. **69**, 1427 (1992).
[3]V. B. Campos, S. Das Sarma, and M. A. Stroscio, Phys. Rev. B **46**, 3849 (1992).
[4]S.-F. Ren and Y.-C. Chang, Phys. Rev. B **43**, 11 857 (1991).
[5]M. A. Stroscio, Phys. Rev. B **40**, 6428 (1989); K. W. Kim and M. A. Stroscio, J. Appl. Phys. **68**, 6289 (1990); K. W. Kim *et al.*, *ibid.* **70**, 319 (1990); M. A. Stroscio *et al.*, Philos. Mag. Lett. **65**, 173 (1992); M. A. Stroscio and K. W. Kim, Phys. Rev. B **48**, 1936 (1993).
[6]M. I. Flik and C. L. Tien, J. Heat Transfer **112**, 872 (1990).
[7]C. Herring, Phys. Rev. **96**, 1163 (1954).
[8]C. L. Tien and J. H. Leinhard, *Statistical Thermodynamics* (Hemisphere, New York, 1979), pp. 307–321.
[9]See, for example, R. Berman, *Thermal Conduction in Solids* (Clarendon Press, Oxford, 1976).
[10]H. B. Casimir, Physica **5**, 495 (1938).